

## REVIEW ARTICLE OPEN

## Materials and corrosion trends in offshore and subsea oil and gas production

Mariano Iannuzzi<sup>1,2</sup>, Afroz Barnoush<sup>1</sup> and Roy Johnsen<sup>1</sup>

The ever-growing energy demand requires the exploration and the safe, profitable exploitation of unconventional reserves. The extreme environments of some of these unique prospects challenge the boundaries of traditional engineering alloys, as well as our understanding of the underlying degradation mechanisms that could lead to a failure. Despite their complexity, high-pressure and high-temperature, deep and ultra-deep, pre-salt, and Arctic reservoirs represent the most important source of innovation regarding materials technology, design methodologies, and corrosion control strategies. This paper provides an overview of trends in materials and corrosion research and development, with focus on subsea production but applicable to the entire industry. Emphasis is given to environmentally assisted cracking of high strength alloys and advanced characterization techniques based on in situ electrochemical nanoindentation and cantilever bending testing for the study of microstructure–environment interactions.

*npj Materials Degradation* (2017)1:2; doi:10.1038/s41529-017-0003-4

## INTRODUCTION

Materials used in oil and gas (O&G) production are exposed to some of the most aggressive industrial environments. Although the rate of serious incidents in the O&G industry is not alarmingly elevated, particularly in the offshore sector,<sup>1</sup> materials degradation could lead to costly catastrophic failures with severe consequence to human life and the environment.<sup>2</sup>

This article discusses the main materials engineering challenges faced in O&G production, illustrating the importance of industry–academia synergies. Emphasis is given to the environmentally assisted cracking (EAC) of high-strength alloys and advanced characterization tools based on in situ electrochemical nanoindentation (ECNI) and cantilever bending. The scope is primarily on offshore and subsea O&G equipment, but most of the topics are equally relevant to up-stream, mid-stream, and down-stream scenarios. Likewise, this article seeks to ignite discussions among industry experts and scholars to help guide future research and development activities.

Although the manuscript presents a comprehensive overview of selected topics, it is not the goal to discuss physical metallurgy and corrosion fundamentals in detail. Readers are encouraged to follow the ample literature provided. There is a myriad of materials and corrosion challenges in O&G production. Interesting subjects such as additive manufacturing, high-strength fasteners, centrifugal casting, corrosion risk management and the industrial internet, cathodic protection (CP) by distributed sacrificial anodes, non-metallic materials and coatings, nano-inspired surface treatments, and many others cannot be addressed herein. The choice of topics is based on the authors' experience and illustrates areas of interest that could have a transformative effect on the business.

## EXTREME ENVIRONMENTS

With conventional O&G reserves dwindling, over the last four decades, the industry has moved towards increasingly more

challenging fields.<sup>3</sup> Although there is not a universal definition differentiating between conventional and unconventional fields, in the context of this publication, unconventional reserves are those that require new materials, design methodologies, and technologies. The most challenging reserves often present high pressures and high temperatures (HPHT), can be in deep-waters (i.e., water depths greater than approximately 800 to 1800 m) or in Arctic regions.<sup>3, 4</sup> Developing HPHT, deepwater, and Arctic prospects at a competitive cost and acceptable risk level is one of the most complex engineering challenges ever faced by the O&G industry.

Although these market segments are technically challenging and require significant capital investment,<sup>5</sup> they have the potential to transform existing technologies and represent the most important source of innovation regarding materials, design methodologies, and corrosion control strategies. This section summarizes the typical environmental conditions that characterize extreme O&G environments.

## High-pressure high-temperature fields

The O&G industry has used different classification criteria to define HPHT conditions over the years. Even today, debate exists as to what constitutes either high pressure or high temperature or both.<sup>6</sup> To standardize the boundaries that characterize HPHT conditions, the American Petroleum Institute (API) has established that HPHT wells are those with:<sup>7</sup>

- Conditions requiring completion and well-control equipment rated at 103 MPa (15,000 psi),
- Shut-in surface pressure above 103 MPa (15,000 psi) or,
- Flowing temperature greater than 177 °C (350 °F).

Despite API's effort to standardize and regulate HPHT developments, some operators and original equipment manufacturers

<sup>1</sup>Norwegian University of Science and Technology (NTNU), Corrosion and Surface Protection, Department of Mechanical and Industrial Engineering (MTP), Faculty of Engineering Science (IV), Trondheim, Norway and <sup>2</sup>General Electric, Oil & Gas, PO BOX 423, Eyvind Lyches vei 10, Sandvika, 1338 Baerum, Norway  
Correspondence: Mariano Iannuzzi (mariano.iannuzzi@ntnu.no)

Received: 6 February 2017 Revised: 7 March 2017 Accepted: 17 March 2017

Published online: 25 July 2017

(OEM) treat HPHT prospects simply as those outside the boundaries of past projects.<sup>8</sup>

The first HPHT onshore well test was drilled in 1965 in the so-called Josephine "A" in Perry County, Mississippi, U.S. HPHT exploration continued during the 1970s, but the trend accelerated with the discovery of the Mobile Bay field in 1981 in offshore Alabama, U.S.<sup>9</sup> Today, the number of HPHT prospects remains marginal when compared with conventional fields; nevertheless, there are active HPHT developments worldwide.<sup>10</sup> Interestingly, HPHT conditions are pervasive in deepwater environments.<sup>11</sup>

HPHT fields can be sweet, i.e., free from hydrogen sulfide ( $H_2S$ ), or sour, i.e. have measurable amounts of  $H_2S$ .<sup>12</sup> Irrespective of their  $H_2S$  concentration, virtually all reservoirs produce carbon dioxide ( $CO_2$ ), with typical levels in the 3–5 vol% range.<sup>13</sup> Both HPHT O&G reservoirs can produce large amounts of water, rich in chlorides and having pH values ranging from nearly neutral to acidic, depending on the characteristics of the geological formation.<sup>14, 15</sup> Likewise, when the  $H_2S$  concentration exceeds 5–10 vol%, elemental sulfur ( $S^0$ ) can be present, increasing the oxidizing power of the water phase and making the field extremely corrosive.<sup>16</sup> Table 1 lists typical alloy families used in O&G production; the following sections elaborate further on the more promising materials for HPHT.

Even though conventional reservoirs can be equally corrosive, HPHT prospects are considered particularly challenging regarding materials performance due to their high pressures, high temperatures, or both.<sup>17</sup> In this regard, EAC and localized corrosion are the prime materials degradation concerns. For instance, the recently released API 17TR8 report mandates EAC testing to quantify the susceptibility of the materials to the environment and to obtain engineering design parameters such as allowable stresses, fracture toughness, and crack-growth rates.<sup>7</sup>

At present, much debate exists regarding the most time- and cost-effective implementation of API's regulations. Furthermore, the industry lacks clear test guidelines to obtain environmental fracture mechanics properties for design purposes.

#### Arctic developments

Independently of the trend towards HPHT fields, O&G exploration and production are moving into Arctic regions.<sup>18</sup> As detailed by Horn et al. and Thaulow and coworkers, the lack of rules and standards for materials selection and qualification has led to much research and development efforts.<sup>18, 19</sup> Components operating in Arctic conditions can be exposed to extremely low temperatures, which requires materials and welds that retain high toughness and fatigue performance at temperatures as low as  $-60\text{ }^\circ\text{C}$ .<sup>20</sup>

### HIGH STRENGTH MATERIALS

High-strength and high-toughness materials with improved fatigue life are desirable, if not essential, to overcome the design challenges imposed by the extreme pressures of HPHT wells and the low temperatures of Arctic regions. Unfortunately, EAC resistance and, in particular, hydrogen assisted cracking performance, decrease with increasing strength.<sup>21</sup> There is, thus, an upper limit for the safe use of engineering alloys in O&G production environments, which is arguably more conservative than in other industries.<sup>22</sup>

There is no universal definition of what constitutes a high strength material, which depends on many factors including the alloy family, the application, and the dimensions or weight of the component. In the context of this article, high strength refers to materials with Specified Minimum Yield Strength (SMYS) values above the typical maximum currently recommended for forged carbon and low alloy steels (LAS) exposed to production fluids, i.e., 550–586 MPa (80–85 ksi).

This section addresses the main limitations of the most common materials used in O&G pressure-retaining equipment and highlights promising research and development trends.

#### Low alloy steels

Contrary to the common perception, LAS are amongst the most advanced engineering materials. By volume, the use of LAS in critical O&G applications far exceeds that of any other alloy family.<sup>23</sup> Therefore, advancements in LAS properties and performance can have a major impact.

Despite their advantages, LAS have, nonetheless, been affected by severe environmentally assisted failures in, e.g.,  $H_2S$ -containing environments and due to hydrogen generated by CP systems.<sup>13, 24</sup> Understanding the underlying mechanisms that lead to adequate EAC resistance, especially in the presence of  $H_2S$ , is paramount.

*LAS for sour service.* From the late 1940's to the end of the 1950's, failures of LAS components related to  $H_2S$  exposure occurred in the U.S., Canada, and France.<sup>25, 26</sup> These events catalyzed research and regulatory work, which ultimately resulted in the publication of the NACE (NACE International, Houston, TX, U.S.) MR0175 standard (i.e., now ISO (International Organization for Standardization, ISO Central Secretariat, 1214 Vernier, Geneva, Switzerland) 15156) in 1975, followed by a major revision in 1978 after a severe fatal accident occurred in Texas, U.S. in 1976.<sup>26, 27</sup>

Most of the early failures were associated with sulfide stress cracking (SSC), at the time a relatively new phenomenon. It is now well known that SSC is a particular form of hydrogen stress cracking (HSC) in the presence of water and  $H_2S$ .<sup>13, 28</sup> As in any other type of HSC, SSC is exacerbated by applied cathodic potentials, but debate still exists concerning the initiation mechanisms under open circuit potential conditions, which are the most relevant in service.<sup>29</sup>

Even though investigators discovered early on that the alloy's microstructure controlled SSC susceptibility,<sup>30</sup> NACE MR0175's approach was to minimize risk by limiting strength and controlling composition, independently of other metallurgical factors. Today, most carbon and LAS are accepted for service under any  $H_2S$  condition if they contain less than 1 wt% nickel and the hardness of the surface exposed to the production fluid is kept below 250HV (22HRC). For example, quenched and tempered (QT) LAS with SMYS values lower than 550 MPa (80 ksi) are believed to resist up to 100%  $H_2S$  when stressed to 100% of their actual yield strength (AYS) at a total pressure of 1 atm.<sup>31</sup>

Carbon steel (CS) and LAS that do not meet strength, hardness, and chemical composition requirements can still be used if successfully qualified. Nevertheless, because testing is costly, complex, and potentially disruptive, OEM and O&G producers typically select materials that meet ISO 15156-2 requirements, avoiding challenging qualification programs.

The hardness limit derives from phenomenological observations showing that SSC was prevented in low strength and softer samples.<sup>26</sup> Hardness is, however, an unreliable estimator of SSC resistance. Indeed, at the same hardness and strength levels, different microstructures exhibited vast differences in EAC susceptibility (Fig. 1).<sup>32</sup> Despite its shortcomings, restricting the hardness of the base metal and the weld drastically reduced the frequency of the early SSC failures. In contrast, the nickel content restriction remains controversial; the work by Kappes et al. could be consulted for a comprehensive review of the topic.<sup>29</sup>

*Moving beyond current limitations.* Cr–Mo steels with SMYS values up to 760 MPa (110 ksi) are typically accepted within the boundaries of ISO 15156.<sup>33</sup> However, because limiting the strength minimizes the risk of exceeding 250HV in weldments, in practice, LAS with SMYS above 550–586 MPa (80–85 ksi) are seldom used for heavy forgings (i.e., cross-sectional thickness

**Table 1.** Nominal composition of representative carbon and low alloy steels as well as CRA for oilfield applications

Alloy designation	Standard nominal composition (wt%)											SMYS MPa (ksi)	
	Cr	Mo	Ni	W	N	Fe	Nb or (Nb + Ta)	Ti (Al)	Cu	C	Si		Mn
Carbon and low alloy steels													
API 5L-X65Q (PSL 2)	-	-	-	-	-	bal.	§	-	-	0.18 (max.)	0.45 (max.)	1.70 (max.)	450 (65)
ASTM A694 F65	-	-	-	-	-	bal.	-	-	-	0.30 (max.)	0.15-0.30	1.60 (max.)	450 (65)
ASTM A508 Gr. 4	1.50 to 2.0	0.40 to 0.6	2.80-3.90	-	-	bal.	-	-	-	0.23 (max)	0.40 (max)	0.20 to 0.40	690 (100)
UNS K32047	1.50 to 1.90	0.50 to 0.65	3.00-3.50	-	-	bal.	-	-	-	0.14 to 0.20	0.15-0.38	0.10 to 0.14	690 (100)
10GN2MFA	0.30 (max.)	0.40 to 0.70	1.80-2.30	-	-	bal.	-	-	-	0.08 to 0.12	0.17-0.37	0.80 to 1.10	414 (60)
UNS K21590	2.00 to 2.50	0.90 to 1.10	0.25 (max)	-	-	bal.	-	-	-	0.11 to 0.15	0.10 (max)	0.30 to 0.60	517-586 (75-85)
UNS G43200	0.40 to 0.60	0.20 to 0.30	1.65-2.00	-	-	bal.	-	-	-	0.17 to 0.22	0.15 to 0.35	0.45 to 0.65	414 (60)
Precipitation-hardened low alloy steels													
ASTM A707-L5	0.60 to 0.90	0.15 to 0.25	0.70 to 1.00	-	-	bal.	-	-	1.00 to 1.30	0.07 (max.)	0.35 (max)	0.09 (max.)	517 (75)
Solution annealed nickel-based alloys													
UNS N06625	20.0 to 23.0	8.0 to 10.0	58.0 (min.)	-	-	5.0 (max.)	(3.15 to 4.15)	-	-	0.10 (max.)	0.50 (max.)	0.50 (max.)	290-414 (42-60) <sup>a</sup>
Precipitation-hardened nickel-based alloys													
UNS N07718	17.0 to 21.0	2.80 to 3.30	50.0 to 55.0	-	-	bal.	(4.87 to 5.20)	0.80 to 1.15	0.23 (max.)	0.045 (max.)	0.010 (max.)	0.35 (max.)	827-965 (120-140)
UNS N07725	19.0 to 22.5	7.00 to 9.50	55.0 to 59.0	-	-	bal.	2.75 to 4.00	1.00 to 1.70	-	0.030 (max.)	0.20 (max.)	0.35 (max.)	827 (120)
UNS N07716	19.0 to 22.0	7.00 to 9.50	59.0 to 63.0	-	-	bal.	2.75 to 4.00	1.00 to 1.60	0.23 (max.)	0.030 (max.)	0.20 (max.)	0.20 (max.)	827-965 (120-140)
UNS N06059	22.0 to 24.0	15.0 to 16.5	bal.	-	-	1.50 (max.)	-	(0.1 to 0.40)	-	-	0.10 (max.)	0.50 (max.)	450 (65ksi) <sup>b</sup>
UNS N06680 <sup>c</sup>	20.5	6.5	bal.	6.5	-	0.1 (max.)	3.5	1.5	-	0.010 (max.)	-	-	550-665 (80-95)
UNS N06686	19.0 to 23.0	15.0 to 17.0	bal.	3.0 to 4.0	-	5.0 (max.)	-	-	-	0.010 (max.)	0.08 (max.)	0.75 (max.)	760 (110) <sup>d</sup>
Duplex and super duplex stainless steels													
UNS S32205	21.0 to 23.0	2.50 to 3.50	4.50 to 6.50	-	0.08 to 0.20	bal.	-	-	-	0.03 (max.)	0.2 to 0.70	2.0 (max.)	450 (65)
UNS S32750	24.0 to 26.0	3.0 to 5.0	6.0 to 8.0	-	0.24 to 0.32	bal.	-	-	-	0.03 (max)	0.8 (max.)	1.2 (max.)	550 (80)
UNS S32760	24.0 to 26.0	3.0 to 4.0	6.0 to 8.0	0.50 to 1.0	0.20 to 0.30	bal.	-	-	0.5 to 1.0	0.03 (max.)	1.0 (max.)	1.0 (max.)	550 (80)
UNS S39274	24.0 to 26.0	2.50 to 3.50	6.0 to 8.0	1.5 to 2.5	0.24 to 0.32	bal.	-	-	0.20 to 0.80	0.03 (max.)	0.8 (max.)	1.0 (max.)	550 (80)
Austenitic and highly alloyed austenitic stainless steels													
UNS S31603	16.0 to 18.0	2.0 to 3.0	10.0 to 14.0	-	-	bal.	-	-	-	0.03 (max.)	1.0 (max.)	2.0 (max.)	182 (27) <sup>e</sup>
UNS S31254	19.5 to 20.5	6.0 to 6.5	17.5 to 18.5	-	0.18 to 0.22	bal.	-	-	0.50 to 1.0	0.020 (max.)	0.80 (max.)	1.0 (max.)	310 (45)
Martensitic and precipitation hardened-martensitic stainless steels													
UNS S41000	11.5 to 13.5	-	-	-	-	bal.	-	-	-	0.15 (max.)	1.0 (max.)	1.0 (max.)	550 (80) <sup>e</sup>
UNS S17400	15.0 to 17.5	-	3.0 to 5.0	-	-	bal.	0.15 to 0.45	-	3.0 to 5.0	0.07 (max.)	1.0 (max.)	1.0 (max.)	724 (105) <sup>f</sup>

§ Ni + V + Ti &lt; 0.15 wt%

<sup>a</sup> Solution annealed<sup>b</sup> ERNiCrMo-13<sup>c</sup> ERNiCrMoWNB-TI-1<sup>d</sup> INCO-WELD-686CPT (Tensile Strength)<sup>e</sup> Double tempered; Hardness 22HRC (max.)<sup>f</sup> H1150-D

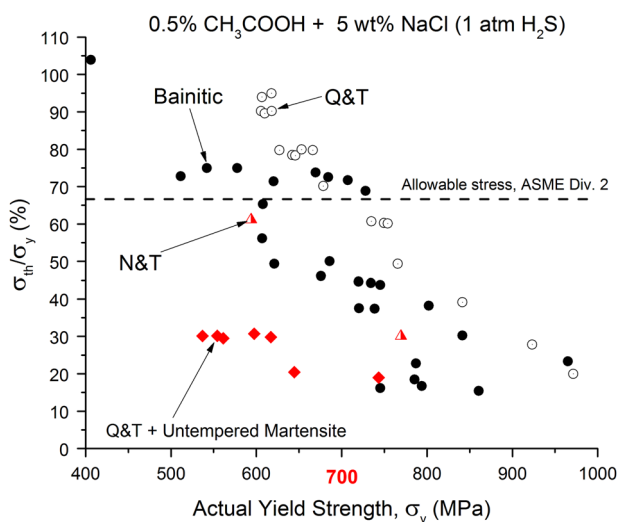


**Fig. 1** Threshold stress ( $\sigma_{th}$ ) of low alloy steels with different microstructures exposed to 0.5 wt%  $\text{CH}_3\text{COOH}$  + 5 wt% NaCl in 1 atm  $\text{H}_2\text{S}$  at 24 °C, normalized to the actual yield strength ( $\sigma_y$ ), versus  $\sigma_y$

above 500–760 MPa). Likewise, ISO 15156's restriction on the allowable nickel content excludes commercial LAS with an exceptional combination of properties such as strength, toughness, weldability, fatigue life, and hardenability.<sup>29</sup> Some LAS such as ASTM (American Society for Testing and Materials, West Conshohocken, PA) A508 Grade 4, 10GN2MF2 and MIL-S-16216K (i.e., a modified version of UNS K32047), Table 1, have been successfully used in hydrogen-bearing atmospheres in, e.g., nuclear reactor pressure vessels.<sup>34</sup> ISO 15156 similarly excludes low-carbon, copper-bearing, precipitation hardenable LAS based on the ASTM A707 specification,<sup>35</sup> which combine high strength, toughness, and weldability (Table 1).<sup>36</sup> Adapting these types of LAS for sour service applications by, for example, reducing their carbon content, tailoring their carbon equivalent, and imposing strict control of the elements responsible for temper embrittlement,<sup>37</sup> could lead to significant weight reductions, improved through-thickness properties, and extended fatigue life.<sup>32</sup>

The safe use of high strength LAS in sour service applications depends primarily on understanding how composition, microstructure, and thermo-mechanical processing affect hydrogen embrittlement (HE) resistance. In this regard, much debate still exists about the influence of the complex microstructures of LAS on SSC and HSC performance. The data compiled by Kappes et al.<sup>29</sup> Fig. 1, suggest that tempered martensite and lower bainite are the most SSC-resistant microstructures based on their threshold stress ( $\sigma_{th}$ ) in  $\text{H}_2\text{S}$ -saturated electrolytes. Normalized and tempered LAS or steels containing fresh martensite are severely affected by hydrogen. Snape has shown that small amounts of untempered martensite have dramatic effects on SSC performance, even on steels that met the macroscopic hardness threshold imposed by ISO 15156.<sup>30</sup> Additionally, Fig. 1 indicates that the threshold stress of QT and bainitic steels was greater than the allowable stress in, e.g., Division 2 of the ASME Boiler and Pressure Vessel Design Code, up to an AYS of about 700 to 750 MPa. The threshold stress decreased rapidly above 750 MPa.

Interestingly, the scatter seen in Fig. 1, particularly on bainitic steels, is associated with the lack of a proper microstructure characterization. Indeed, most authors did not specify the type of bainite, i.e., upper or lower, or martensite, i.e., plate, lath, or a combination, and some assumptions had to be made based on the reported heat treatment procedures and alloy compositions to construct Fig. 1. Even today there are critical aspects of the bainitic and martensitic phase transformations in steels, such as the

carbide precipitation mechanisms, that remain unresolved and, according to some authors, might hold up technological progress.<sup>38, 39</sup>

Even though experimental observations have shown that the alloy's microstructure determines SSC and HSC resistance, researchers have yet to agree on a mechanistic explanation. Phenomenological observations speculate that the high residual strain associated with untempered martensite, the presence of carbides at GB in upper bainite needles, and the type of ferrite-carbide interface in ferritic-pearlitic alloys could facilitate hydrogen-dislocation interactions.<sup>32</sup>

There seem to be a renaissance in LAS research, specially bainitic LAS, with high- and ultra-high strength, fueled in part by industry-academic synergies.<sup>40</sup> Researchers have recently developed, e.g., commercial oil country tubular goods (OCTG) with SMYS values up to 860 MPa (125 ksi) that resist SSC in mild and intermediate sour service conditions<sup>41</sup> thanks to advancements in grain boundary engineering.<sup>42–45</sup> The authors have found that the high dissipation energy of special high-angle grain boundaries (GB), i.e. more than 30°, reduced the driving force for crack propagation. Figure 2 presents the qualitative distribution of special GB obtained by electron backscatter diffraction (EBSD). The ideal amount and distribution of special GB depend not only on the final QT heat treatment but also on the austenitization step. This example illustrates the importance of metallurgical design in obtaining high strength LAS with adequate EAC resistance. Future investigations on richer LAS compositions for heavy forged sections will benefit from advancements in this area.

#### Precipitation hardened (PH) corrosion resistant alloys (CRA)

As a rule of thumb, large-bore (i.e., an internal diameter greater than approximately 50 cm) subsea production components, such as valves, connectors, and pipes, are commonly made of LAS overlaid or clad with a CRA.<sup>46</sup> Full-clad or partially-clad designs take advantage of the strength and low cost of the LAS core, whereas the CRA inlay minimizes the corrosion concerns associated with LAS exposure to aqueous electrolytes containing  $\text{CO}_2$  and  $\text{H}_2\text{S}$ .<sup>47</sup> In subsea O&G production, LAS are typically weld overlaid with UNS N06625 (NA625), a nickel-based seawater resistant CRA (Table 1), but different stainless steels and nickel alloys could be used.<sup>22</sup> Despite the fact that the surface exposed to production fluids is made of a CRA, the base LAS has to comply with the strength, hardness, and alloy chemistry requirements of ISO 15156.

PH CRA are used when the application requires strength levels exceeding the limits imposed by ISO 15156 on LAS, i.e., SMYS above 690–760 MPa (100–110 ksi). Both stainless steel and nickel-based PH alloys find numerous applications in O&G production. In particular, PH nickel-based alloys (PHNA) are extensively used in wellbore components due to their combination of strength and EAC resistance.<sup>48</sup> Whereas all PHNA can sustain the most aggressive production environments, not all PHNA families are seawater resistant.<sup>49</sup>

The most common PHNA is UNS N07718 (NA718), a super nickel alloy containing 17–21 wt% Cr, 2.8–3.3 wt% Mo, 50–55 wt% Ni, Nb, Ta, and Ti (Table 1).<sup>50</sup> NA718 was first developed for high-temperature aerospace applications, and introduced in the O&G industry in the early 1980s.<sup>48</sup> NA718 is strengthened by an ordered, body-centered tetragonal  $\gamma''$  phase, and an ordered face-centered cubic  $\gamma'$  phase.<sup>51</sup> Despite its excellent performance in sour production environments, NA718 suffers pitting and crevice corrosion in oxidizing halide-containing environments due to its intermediate Cr and Mo content. Indeed, NA718 has a localized corrosion performance similar to that of stainless steels of comparable Cr and Mo such as UNS S31600, Table 1.<sup>52</sup>

Alloys UNS N07725 (NA725) and UNS N07716 (NA716) are frequently selected when the application requires improved

localized corrosion performance (Table 1). Both PHNA derived from NA625 and, like NA718, are strengthened by  $\gamma'$  and  $\gamma''$  phase.<sup>53, 54</sup> NA725 and NA716 can resist the most aggressive sour environments and are considered seawater resistant per ISO 21457,<sup>46</sup> based on their Pitting Resistance Equivalent.<sup>54, 55</sup> Currently, no standard defines the maximum allowable temperature for seawater service of NA725 and NA716; nevertheless, NA625 is restricted by ISO 21457 to 30 °C due to crevice corrosion concerns in chlorinated systems.

While it is well established that the presence of  $\delta$ -phase severely compromises NA718's HSC and SSC resistance,<sup>56</sup> PHNA have been, a priori, considered immune to hydrogen embrittlement in the age-hardened conditions used in O&G applications.<sup>48</sup> However, sudden cleavage failures of NA718,<sup>57</sup> NA716,<sup>58</sup> and NA725<sup>59</sup> subsea components in relatively benign environments have been reported during installation and operation, all associated with HE. Figures 3 and 4 illustrate a recent EAC intergranular cleavage failure of an NA725 part. While in these failures the hydrogen source has not always been well established, it is suspected that H from either CP, electroplating, galvanic coupling to carbon steel, or from degradation of non-production fluids could have played a role.<sup>60</sup> More alarmingly, in most instances, materials and manufacturing processes met international specifications, suggesting that existing best practices do not capture all the variables that lead to an optimal microstructure.

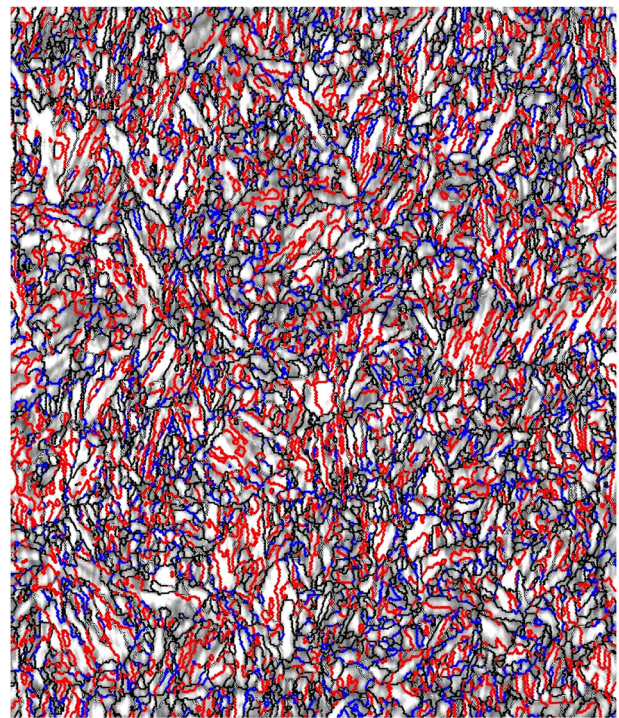
In the example shown in Figs. 3 and 4, the precipitation of a continuous network of a nano-sized topologically close-packed (TCP) phase (i.e.,  $\sigma$ -phase in this case) along GB may have led to HSC. Figure 4 shows the degree of GB coverage by  $\sigma$ -phase, which was 90 to 100%, and secondary crack propagation along the matrix/ $\sigma$ -phase interface. GB decoration was visible in the scanning electron microscope (SEM) after special sample preparation steps and could be characterized only by transmission electron microscopy (TEM). It is unclear whether the formation of  $\sigma$ -phase is possible in the temperature and time ranges allowed in existing standards but impossible to be detected up to now; or if residual strain introduced during thermo-mechanical processing could accelerate precipitation kinetics well below the 30 h reported by Mannan<sup>53</sup> and Oradei-Basile.<sup>51</sup> Moreover, despite the evidence suggesting the deleterious effect of TCP phases, their role in EAC and the mechanisms involved are still unclear. The O&G industry will benefit from multi-disciplinary research activities aimed at elucidating the processing and manufacturing parameters that result in TCP precipitation and the mechanisms leading to EAC.

## Welding

Since most pressure-containing components must be welded, weldability is one of the most important technological properties in the design of O&G equipment. Thus, increasing the strength of the base material requires a filler metal with comparable or better mechanical properties. The necessity of joining dissimilar metals, particularly clad LAS to stainless steels, exacerbates the challenge.

Welding and cladding of dissimilar materials are commonplace in the subsea O&G industry. A typical example is the joining of austenitic and duplex or super duplex stainless steels (DSS and SDSS, respectively) to carbon or LAS, which can be either bare or clad. The current approach is to use niobium-free nickel-based CRA, e.g., UNS N06059 or UNS N06686 (Table 1), as a filler material to prevent the hydrogen-related cracking of NA625-butted joints that has affected subsea production components.<sup>61, 62</sup>

When following present welding procedures, lean LAS compositions such as API 5L<sup>63</sup> Grade up to X65, and ASTM A694 (ref. 64) up to F65 do not require post-weld heat treatment (PWHT). In contrast, richer chemistries, such as UNS K21590 (ASTM A182 F22),<sup>65</sup> are conventionally buttered with a 1%Ni-½%Cr LAS filler metal (e.g., American Welding Society, Miami, FL) A.23:EG or EN



Boundary levels:  
40.00  $\mu\text{m}$  = 80 steps IQ -20...140

**Fig. 2** Qualitative distribution of special grain boundaries ( $\Sigma$ : 3 in red,  $\Sigma$ :11, 25b, 33c and 41c in blue) in a QT pipeline steel obtained by electron backscatter diffraction. Image Courtesy of Tenaris

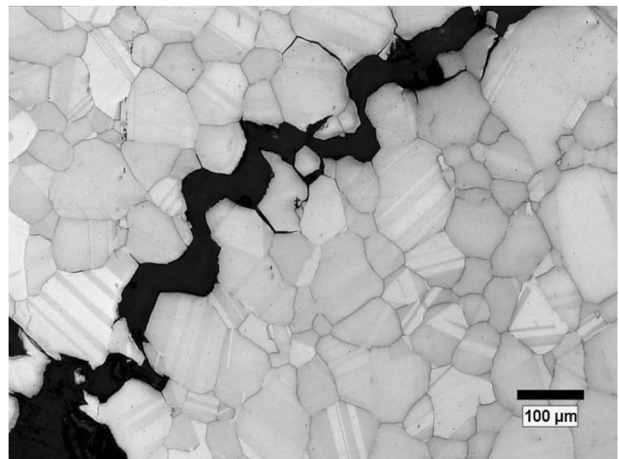


**Fig. 3** Hydrogen embrittlement of UNS N07725 showing signs of intergranular cleavage. Image courtesy of General Electric

(European Standard, European Committee for Standardization, Brussels, Belgium) 756: S3NiMo1), and heat treated before welding to the stainless steel part.<sup>66</sup> Heat treating the buttered section before joining prevents sensitization during PHWT of, e.g., DSS and SDSS components.<sup>67</sup>

At present, the highest strength of dissimilar weld joints is controlled by the SMYS of the nickel-based CRA filler to about 470 MPa (68 ksi). Although some researchers recommended under-matching the strength of the consumables used to weld high strength LAS,<sup>68</sup> this practice is discouraged by current design codes.<sup>69</sup> Therefore, the SMYS of the base metal is restricted to a

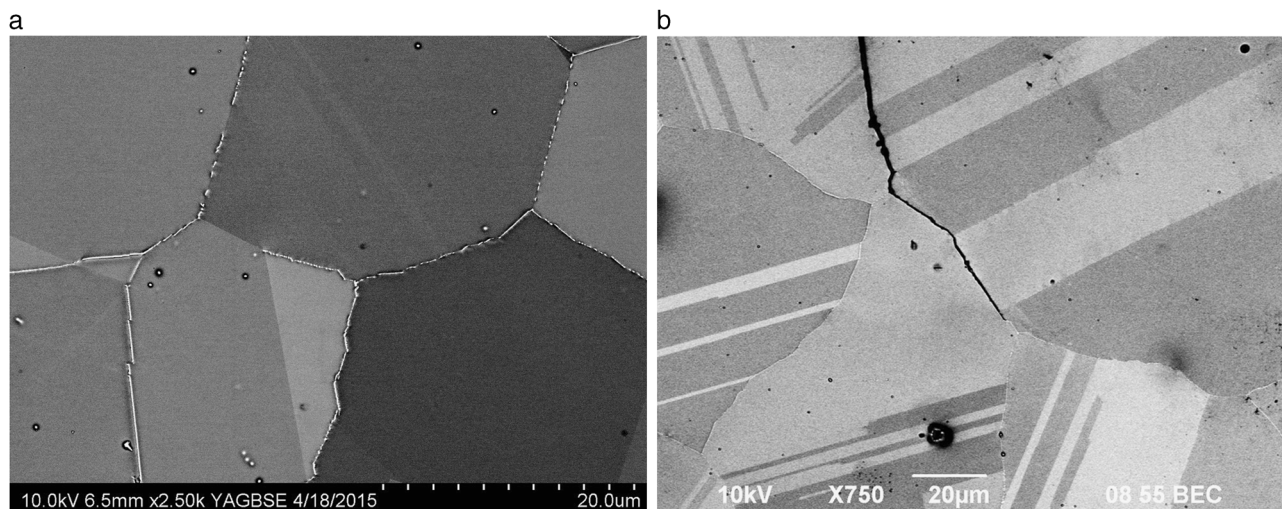


**Fig. 4** Microstructure characterization of the affected UNS N07725 samples: **a** almost full grain boundary coverage by a topologically close-packed phase (TCP), and **b** secondary HE cracking propagating along the matrix-TCP interface. Images courtesy of General Electric

slightly lower strength, to prevent making the weldment the weaker part of the joint.<sup>70</sup>

Mannan and coworkers have recently introduced a new PH nickel-based Ni–Cr–Mo–W–Nb–Ti filler metal designated as UNS N06680 (NA680), Table 1.<sup>71</sup> According to the authors, NA680 can be used to weld clad-OCTG with an SMYS, in the as welded condition, of up to 550 MPa (80 ksi). The alloy can reach high strength levels due to self-aging or auto-aging during cooling. Nevertheless, the AYS of the joint was strongly affected by the heat input of the process. The maximum reported yield strength was about 655 MPa (95 ksi) but, in some instances, it did not reach 550 MPa (80 ksi). Despite the promising results presented by Mannan and coworkers, there are no universally accepted practices to weld clad-LAS with SMYS above approximately 450 MPa (65 ksi) to stainless steels. The successful introduction of high-strength LAS in subsea O&G equipment will, in a great measure, depend on the development of high strength filler metals and new welding procedures.

### PUSHING THE LIMITS OF CRA

A multitude of CRA are used in oilfield applications, including martensitic, austenitic, ferritic, duplex, and PH stainless steels, solution annealed and PHNA, as well as titanium, cobalt, and aluminum alloys. Examples of typical CRA are shown in Table 1. Materials selection of CRA is primarily governed by part 3 of the ISO 15156 standard (ISO 15156-3)<sup>26</sup> and ISO 21457.<sup>46</sup> The scope of the ISO 15156-3 specification includes clearly opposing mechanisms such as stress corrosion cracking (SCC), SSC, and galvanically-induced hydrogen stress cracking (GHSC). The philosophy of ISO 15156-3 is to set strict limits on the parameters that influence these forms of corrosion; i.e., the partial pressure of H<sub>2</sub>S, solution pH, chloride concentration, temperature, and the presence or absence of S<sup>0</sup>. Likewise, ISO 15156-3 restricts strength and hardness in certain alloy systems. The materials' boundaries established by the standard derive from a combination of industry experience and qualification testing and have been initially resisted by the industry.<sup>14, 72</sup>

One of the chief criticisms to ISO 15156-3 is that it represents a “one-size-fits-all” approach to materials selection. Thus, exceeding one of the environmental limits presented in Annex A of the standard implies that (i) the chosen alloy is unfit for service or (ii) the alloy requires additional qualification testing. Annex B details the recommended qualification testing procedures. However, the testing methodology, the exposure conditions, the extent of

validity (i.e., per heat, heat treatment lot, manufacturer, etc.), as well as the essential variables that trigger re-qualification must be agreed upon by the operator, the OEM, and the alloy producer. In practice, because qualification testing is costly and time-consuming and, as importantly, because no clear quality control practices exist to certify materials during production, designers typically avoid testing altogether and opt for a more resistant CRA instead. Interestingly, this approach is currently being challenged by the API 17TR8 Task Group, which has specified comprehensive EAC testing for HPHT applications in simulated production environments, seawater with CP, as well as corrosive non-production fluids.<sup>7</sup>

Irrespective of any criticism to the degree of conservatism in ISO 15156-3 Annex A,<sup>22</sup> the broad scope of the standard is questionable. GHSC, i.e., a form of HSC in which nascent H is produced at the CRA surface due to galvanic coupling to a less resistant alloy,<sup>28</sup> and SSC are exacerbated at lower temperatures than those observed in the wellbore near the reservoir. Because GHSC can occur in the absence of uniform or localized corrosion of the CRA, a material could meet ISO 15156-3 restrictions regarding environmental conditions and maximum allowable temperature, yet be susceptible to GHSC if subjected to galvanic coupling. In this regard, high strength alloys such as martensitic stainless steels are particularly susceptible to GHSC.<sup>73</sup>

ISO 15156-3 mandates GHSC testing to ballot new materials for inclusion in the standard. However, not all materials listed in the specification have been evaluated for GHSC. In such instances, the boundaries were established based on industry experience.<sup>14</sup> Lastly, it is important to emphasize that SSC of CRA can only occur below the depassivation pH (pH<sub>d</sub>), which for many of the higher grade CRA can be as low as 1.<sup>74</sup> Given the recent HSC failures of PHNA,<sup>57–59</sup> which are amongst the most resistant materials listed in ISO 15156-3, in relatively benign conditions, it is strongly advisable that the ISO and NACE maintenance committees revisit the implications of the current extent of the standard.

In contrast to SSC and GHSC, SCC is an anodic process mainly controlled by the stability of the passive film and the local chemistry. Researchers have found that pitting corrosion appears to be a prerequisite for SCC in production environments, as the conditions that stabilize a pit are similar to those required for SCC.<sup>75, 76</sup> Anderko, Sridhar and coworkers have developed a framework that uses the repassivation potential ( $E_{RP}$ ) and the corrosion potential ( $E_{COR}$ ) to estimate the likelihood of SCC in sour production environments.<sup>77–79</sup> The main assumption is that SCC occurs only in the presence of localized corrosion when the

temperature is above the critical pitting temperature and  $E_{\text{Corr}} > E_{\text{RP}}$ . The authors have validated a quantitative model that predicts both  $E_{\text{RP}}$  and  $E_{\text{Corr}}$  of martensitic stainless steels as a function of solution chemistry and temperature.<sup>78, 79</sup>

The approach developed by Anderko et al. has tremendous potential as it could be used to revise ISO 15156-3 limits and optimize materials selection. Additionally, the combination of a robust quantitative model and, e.g., sensors could be implemented in new corrosion risk management tools. For example, reference electrodes added to oilfield equipment could monitor  $E_{\text{Corr}}$  over time.  $E_{\text{Corr}}$  data could, then, be compared to  $E_{\text{RP}}$  values, estimated as a function of the actual composition of the produced fluids. More research is needed to extend the approach to other CRA families, in particular, DSS and SDSS since their current environmental boundaries are perceived as being excessively conservative.<sup>80</sup>

#### Effect of hydrogen on the localized corrosion resistance of CRA

Although hydrogen generated by either corrosion or by CP has been shown to deteriorate the protectiveness of passive films, existing EAC models do not take this effect into consideration. Yao et al.,<sup>81</sup> Guo et al.,<sup>82</sup> Pyun et al.,<sup>83, 84</sup> Thomas et al.,<sup>85</sup> Armacanqui and Oriani,<sup>86</sup> to name a few, have shown that in part due to its strong reducing properties, hydrogen present in the passive film lowers the resistance to pitting corrosion. Yao et al. attributed the decrease in localized corrosion resistance of UNS S32205 to a change in the semiconductor properties of the chromium oxide film.<sup>81</sup> The authors showed that  $E_{\text{Corr}}$  decreased and the passive current density increased due to pre-charging. Similar results were also seen by Thomas et al. on CS.<sup>85</sup> Interestingly, anecdotal evidence from recent failure investigations on SDSS seawater pumps seems to confirm the deleterious effect of hydrogen on localized corrosion resistance. In this regard, severe localized corrosion was found after removal of the CP system under conditions a priori benign to SDSS. The recent work by Thomas et al.<sup>87</sup> can be consulted for a more comprehensive overview of the role of hydrogen on corrosion of CS and LAS, as well as CRA.

More research is needed to comprehend the influence of hydrogen on localized corrosion resistance fully and, consequently, its influence of EAC. In this regard, the presence of  $\text{H}_2\text{S}$  could further complicate the issue as the effect of H on, e.g.,  $\text{Fe}_{1+x}\text{S}$  films has yet to be investigated. However, the marked decrease in  $E_{\text{Corr}}$  and the increase in passive current density reported for stainless steels and CS open the door to in situ corrosion monitoring techniques. It is plausible to envision, for example, a simple  $E_{\text{Corr}}$  monitoring device that, when coupled to proper corrosion models, could be used to determine localized corrosion and EAC risks.

#### ON THE TRAIL OF HYDROGEN

Industry-academia synergies are essential to overcome the challenges discussed in previous sections. Methodologies based on SEM and TEM, focused ion beam (FIB), as well as atomic force microscopy, coupled with in situ micro-mechanical and nano-mechanical and electrochemical techniques have matured rapidly over the last decade. Today, researchers have at their disposal an exceptional toolkit that allows multi-scale characterization, from the nanoscale to full-size industrial settings, of complex phenomena like HE.<sup>88</sup> The combination of approaches is helping shed new light on the compound microstructure-environment interactions leading to EAC. This section discusses recent advancements in hydrogen embrittlement research with a focus on ECNI, nano-mechanical characterization, and electrochemical microcantilever bending.

#### Hydrogen effects in metals: an elusive phenomenon

Hydrogen is the smallest atom in the universe, and its small size makes it a controversial interstitial in comparison to the other common interstitial atoms. While all other interstitial elements, e.g., C, N, and B seem to have beneficial effects on the mechanical properties of metals and, more specifically, steels, the presence of H results in a severe degradation of strength and toughness. A recent ab initio simulation shows that the small size of the H atom in the crystal lattice results in the formation of nonsymmetrical bonds between H and the host metal atoms.<sup>89–91</sup> Additionally, H is a mobile interstitial at room temperature. Apart from the complications arising from the H uptake and transport processes in the metal, the interaction of the dissolved H atom with the crystal lattice and crystal defects, e.g., dislocations and GB, and consequently its effect on mechanical properties is a highly-complicated process. Traditionally, conventional macro-scale mechanical tests have been used to study the effect of dissolved hydrogen on the mechanical behavior of metals and alloys. However, it is almost impossible to decouple such macroscopic tests from the H uptake and transport processes. Moreover, a conventional test measures the response of a macroscale sample

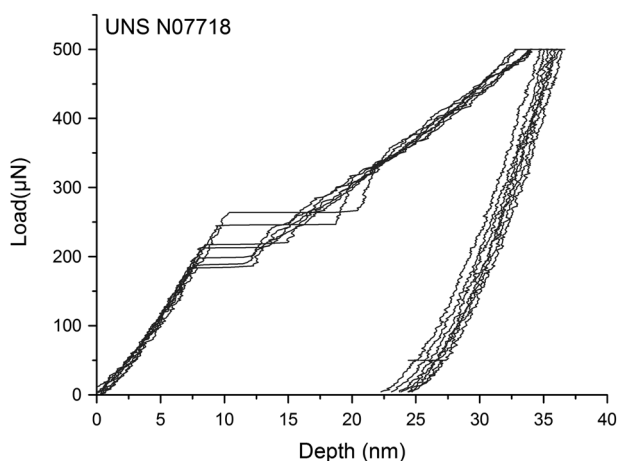


**Fig. 5** Load-displacement curves resulting from nanoindentation on UNS N07718 in the aged hardened condition. Clear pop-ins in the range of 190 to 270  $\mu\text{N}$  are observed

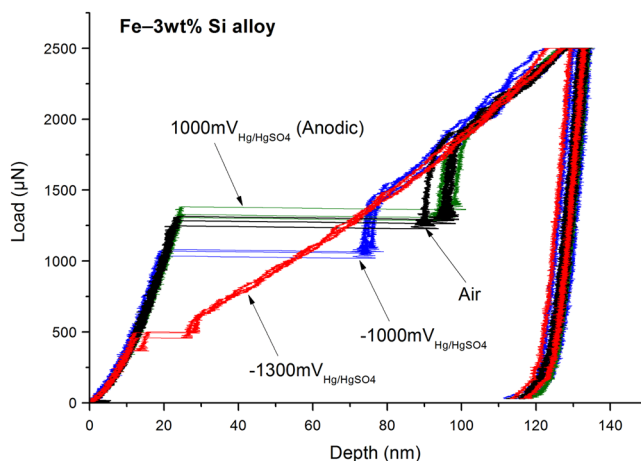


**Fig. 6** Effect of applied potential on dislocation nucleation in a model Fe-3 wt% Si alloy. Applied potentials as indicated. For the green curve, the applied potential was switched to 1000  $\text{mV}_{\text{Hg}/\text{HgSO}_4}$  in the anodic direction after an initial cathodic polarization of  $-1000 \text{ mV}_{\text{Hg}/\text{HgSO}_4}$ , followed by a cathodic polarization of  $-1300 \text{ mV}_{\text{Hg}/\text{HgSO}_4}$

8 to a mechanical load, while the H interaction with the lattice is a discrete localized process distributed over time and space. H effects take place in specific H-enriched locations of the sample. In other words, the signal to noise ratio in macroscopic tests is

considerably low. Undeniably, very useful qualitative information and design parameters can be extracted from conventional tests; however, a mechanistic understanding of the HE phenomenon requires tools with a higher signal-to-noise ratio. A typical, but not trivial, approach is, thus, to reduce the size of the sample and perform micro- and nanoscale mechanical evaluations.<sup>92–95</sup>

#### Challenges of small-scale testing

Once the size of the specimen or the volume of the material is reduced, the most challenging task is to retain the H atoms in such small dimensions. Except for some special alloys and metals,<sup>96, 97</sup> it is impossible to stop hydrogen outgassing from a small sample. Therefore, a microscale mechanical evaluation of the influence of H in mechanical properties should be combined with in situ H charging.

#### Studying hydrogen-dislocation interactions: ECNI

Undoubtedly, nanoindentation has been the most popular and frequently used small-scale testing method over the last decades.<sup>98</sup> Combined with scanning probe microscopy and imaging capabilities with the same tip used for indentation; nanoindentation is a unique mechanical testing method that provides a high-resolution characterization.<sup>99</sup>

A typical nanoindentation test consists of several steps. First, after imaging the surface topography, the tip can be located with

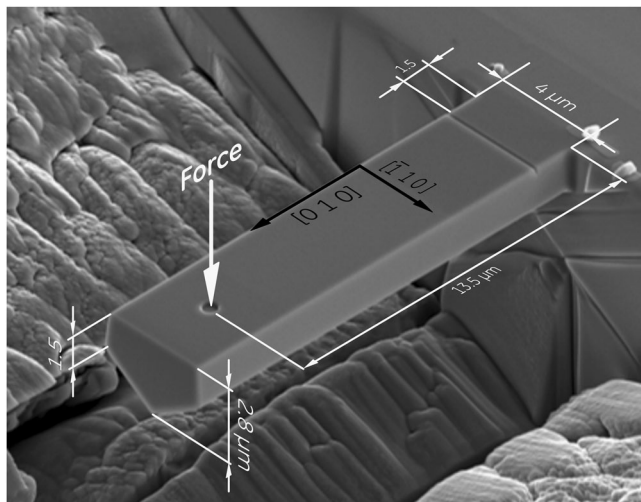


**Fig. 7** Microcantilever geometry and dimensions

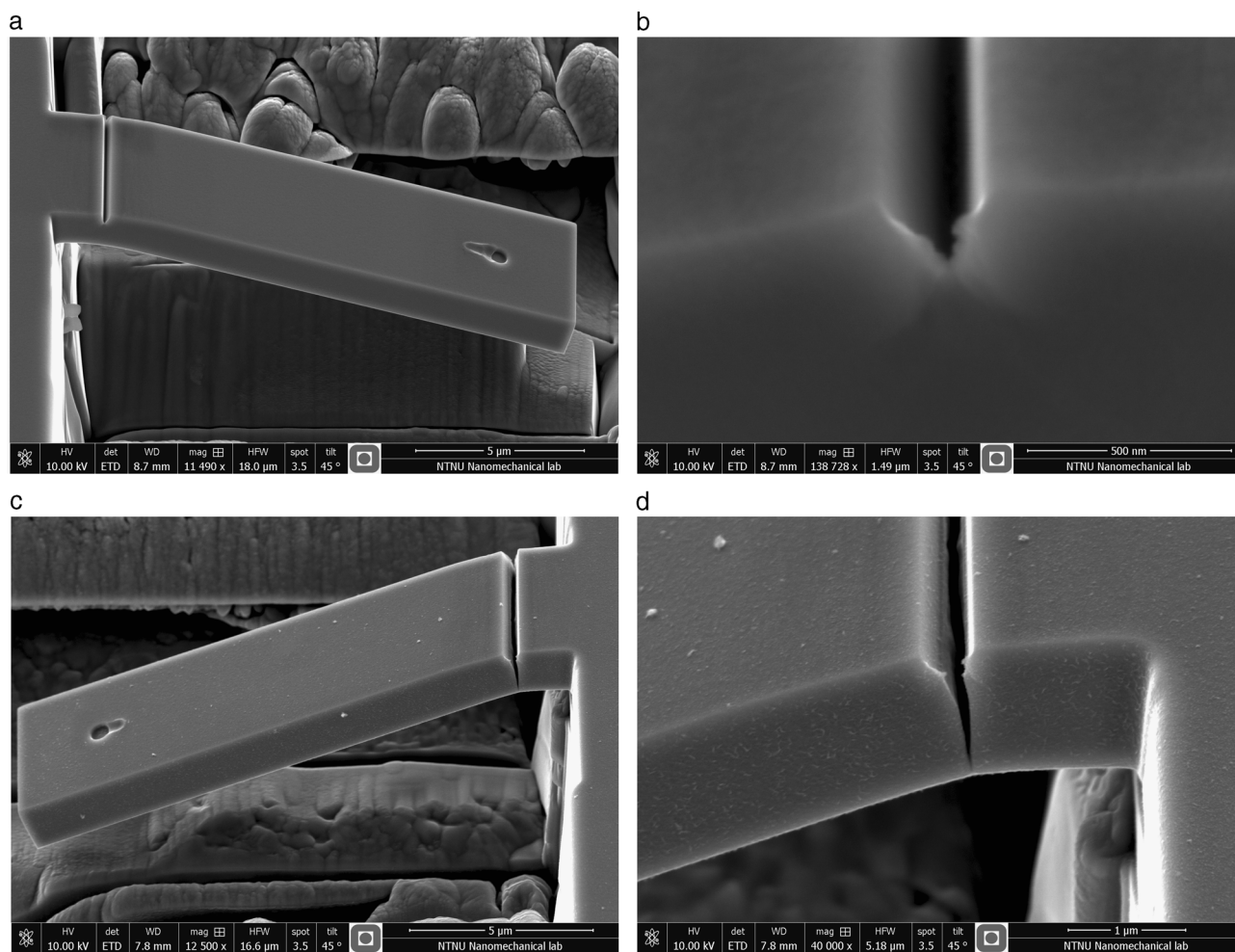


**Fig. 8** In situ microcantilever bending of Fe-3 wt% Si: **a** cantilever bent in air, **b** higher magnification micrograph of the root of the FIB notch bent in air, **c** H-charged cantilever bent in the electrolyte under cathodic polarization, and **d** higher magnification micrograph of the root of the FIB notch (H-charged)



nanometer precision. Subsequently, multiple indentations can be performed while registering the indentation load and displacement of the tip. In well-prepared samples with low dislocation density, the probability of indenting a dislocation-free region is very high. In such instances, the indentation starts with an elastic loading that follows the Hertzian contact model.<sup>100–106</sup>

As the shear stress below the tip in the volume of the material approaches the theoretical stress required for homogeneous dislocation nucleation, a sudden jump, i.e., the so-called pop-in, in the displacement occurs. The pop-in marks the transition from elastic to elastoplastic deformation in a perfect crystal. Then, the indentation continues in the elastoplastic regime up to the maximum indentation load. The unloading curve can be assumed to be fully elastic and is typically used to extract the hardness and elastic modulus of the material per the Oliver–Pharr method.<sup>107</sup> Typical load-displacement curves of NA718 are shown in Fig. 5.

ECNI combines nanoindentation with in situ electrochemical hydrogen charging. ECNI provides distinct possibilities for studying the influence of H on mechanical properties, especially the effect of hydrogen on dislocation nucleation. The results of in situ ECNI on a research-grade Fe–3wt.% Si alloy, Fig. 6, show that the required load for pop-in, i.e., homogeneous dislocation nucleation, is reduced in the presence of H. Additionally, the amount of the reduction in the pop-in load scales with the amount of hydrogen which is controlled by the applied electrochemical polarization. Per the defactant theory,<sup>108–111</sup> the decrease in the load required for dislocation nucleation can be related to the reduction in the dislocation line energy by H.<sup>96, 112, 113</sup>

Hydrogen effects on crack propagation: microcantilever bending tests

FIB cut micro-samples, loaded inside a nanoindenter equipped with special tips have traditionally been used to study size-effects in metals and alloys.<sup>114–118</sup> The possibility of in situ electrochemical H charging inside a nanoindenter provides a unique opportunity to perform such microscale experiments on H-charged samples, Fig. 7.

Figure 8 shows a cantilever cut in a Fe–3 wt% Si model alloy after bending in air and under continuous H charging. The presence of hydrogen resulted in the nucleation of a crack at the root of the notch in the beam. Postmortem high-resolution sub-microstructural examination, e.g., EBSD<sup>93</sup> and TEM<sup>92</sup> could be performed on these cantilevers to reveal the mechanism of hydrogen embrittlement at the dislocation level.

Presently, in situ microcantilever bending has been successfully applied to relatively simple model materials and monocrystalline microcantilevers. In the future, alloys with more complex microstructures, e.g., PH-CRA, as well as bi-crystalline cantilevers will be used to study the role of different microstructural features during the hydrogen embrittlement process and their interaction with the crack tip in the presence of hydrogen.

## CONCLUSIONS

High strength materials, including LAS and PH-CRA, are essential to overcome the materials hurdles associated with the production of hydrocarbons from unconventional reservoirs.

EAC and localized corrosion are the two primary degradation forms that affect the alloys required for the safe and economic operation of sour, HPHT, and Arctic fields. A better understanding of the metallurgical factors and manufacturing variables that lead to optimal EAC resistance is paramount.

In situ characterization techniques, such as ECNI and microcantilever bending, can provide unique insights into the crack initiation and propagation mechanisms. Nevertheless, much research is still required to extend the findings of nano-scale

and micro-scale testing to the macroscopic corrosion performance of engineering alloys.

Strengthening the close collaboration between industry and academia is essential to develop a multi-scale understanding of the compound microstructure–environment interactions to lead to optimal EAC resistance.

## ACKNOWLEDGEMENTS

The authors thank Atle H. Qvale (General Electric, Oil & Gas) and Dr. Martin Morra (General Electric, Global Research Center), as well as Dr. María José Cancio (Tenaris) for their invaluable contribution and discussions. We would also like to thank Prof. Nick Birbilis for his encouragement and for inviting us to submit our work. General Electric and the Norwegian University of Science and Technology sponsored the publication of this manuscript equally. We thank the support of the Research Council of Norway to the NTNU NanoLab through the Norwegian Micro-Fabrication and Nano-Fabrication Facility, Norfab (197411/V30) and projects HIPP (234130/E30) and HyF-Lex (244068/E30).

## AUTHOR CONTRIBUTIONS

All authors contributed equally to this manuscript.

## ADDITIONAL INFORMATION

**Competing interests:** The authors declare no competing financial interests

**Publisher's Note:** Springer Nature remains neutral with regard to jurisdictional claims in published maps and institutional affiliations.

## REFERENCES

1. U.S. Bureau of Labor Statistics. Employer-reported workplace injuries and illnesses–2015. Report No. USDL-16-2056, (Washington, D.C., 2016).
2. U.S. Chemical Safety and Hazard Investigation Board. Investigation report volume 2-Explosion and fire at the Macondo well. Report No. 2010-10-I-OS, (Washington, D.C., 2014).
3. Bell, J. M., Chin, Y. D. & Hanrahan, S., State-of-the-Art of Ultra Deepwater Production Technologies. in *Offshore Technology Conference*, 2–5 (Society of Petroleum Engineers, 2005).
4. Iannuzzi, M. in *Stress Corrosion Cracking. Theory and Practice* (eds Raja, V. S. & Shoji, T.) Ch. 15, 570–607 (Woodhead Publishing, 2011)
5. Michie, D. Economic Report 2016 (Oil & Gas, London, U.K., 2016).
6. Skeels, H. B. API 17TR8-HPHT Design Guideline for Subsea Equipment. in *Offshore Technology Conference*, OTC-25376-MS (Houston, TX, Offshore Technology Conference, 2014).
7. API 17TR8, *High-pressure High-temperature Design Guidelines* (American Petroleum Institute, 2015).
8. Kfoury, M. *Kristin HPHT Gas Condensate Field: challenges, remedial actions & strategy to improve hydrocarbon reserve* (Statoil AS, 2012).
9. Lehr, D. J. & Collins, S. D., The HPHT Completion Landscape-Yesterday, Today, and Tomorrow. in *SPE Annual Technical Conference and Exhibition*, SPE-170919-MS, 27–29 (Society of Petroleum Engineers, 2014).
10. Avant, C. et al. Testing the limits in extreme well conditions. *Oilfield Rev.* **24**, 4–19 (2012).
11. Mazerov, K. HPHT completions: always a moving target. *Drill. Contractor* (2011). <http://www.drillingcontractor.org/hpht-completions-always-a-moving-target-9344>.
12. NACE/ASTM G193–12d, *Standard Terminology and Acronyms Relating to Corrosion* (ASTM International, 2012).
13. Wilhelm, S. M. & Kane, R. D. Selection of Materials for Sour Service in Petroleum Production. *J. Pet. Technol.* **38**, 1051–1061 (1986).
14. NACE International Work Group T-1F-21G. Use of Corrosion-Resistant Alloys in Oilfield Environments. Report No. 1F192, (NACE International 2000).
15. European Federation of Corrosion. *Guidelines on Materials Requirements for Carbon and Low Alloy Steels for H<sub>2</sub>S-Containing Environments in Oil and Gas Production*. 3rd edn., Vol. Publication No. 16 (Maney Publishing, 2009).
16. Smith, L. & Craig, B. D., Practical corrosion control measures for elemental sulfur containing environments. in *CORROSION 3–7* (NACE International, 2005).
17. Walton, D., Equipment and material selection to cope with high pressure/high temperature surface conditions. in *Offshore Technology Conference*, OTC-12122-MS (Offshore Technology Conference, 2000).

18. Horn, A. M., Østby, E., Hauge, M. & Aubert, J.-M. in *The Twenty-second International Offshore and Polar Engineering Conference* 290–296 (International Society of Offshore and Polar Engineers, 2012).
19. Thaulow, C., Ødegård, J. & Østby, E., Arctic steels criteria for safe materials utilisation. in *High Technologies in Advanced Metal Science and Engineering* (St. Petersburg, Russia, 2006).
20. Alvaro, A., Akselsen, O. M., Ren, X. & Kane, A. in *Proceedings of the Twenty-fourth International Ocean and Polar Engineering Conference* 247–254 (International Society of Offshore and Polar Engineers, 2014).
21. Gangloff, R. P. in *Comprehensive Structural Integrity* Vol. 6 (eds Milne, I., Ritchie, R. O. & Karihaloo, B) Ch. 6.02, 31–101 (Elsevier Science, 2003).
22. Rhodes, P. R., Skogsberg, L. A. & Tuttle, R. N. Pushing the limits of metals in corrosive oil and gas well environments. *Corrosion* **63**, 63–100 (2007).
23. Davenport, E. S., Fundamental Characteristics of Alloy Steel. in *Drilling and Production Practice*, API-35-209, 209–225 (American Petroleum Institute, 1935).
24. Craig, B. D. On the contradiction of applying rolled threads to bolting exposed to hydrogen-bearing environments. *Oil Gas Facilities* **4**, 66–71 (2015).
25. Vollmer, L. W. Hydrogen sulphide corrosion cracking of steel. *Corrosion* **8**, 326–332 (1952).
26. Milliams, D. E. & Tuttle, R. N., ISO 15156/NACE MR0175-A new international Standard for metallic materials for use in oil and gas production in sour environments. in *CORROSION*, 03090, 16–20 (NACE International, 2003).
27. Craig, B. D. in *Sour-gas design considerations SPE Monograph Series* Ch. 1, 1–3 (Society of Petroleum Engineers, 1993).
28. ISO 15156 (1–3), *Petroleum and natural gas industries - Materials for use in H2S-containing environments in oil and gas production* (International Organization for Standardization, 2015).
29. Kappes, M., Iannuzzi, M., Rebak, R. B. & Carranza, R. M. Sulfide stress cracking of nickel-containing low-alloy steels. *Corros. Rev.* **32**, 101–128 (2014).
30. Snape, E. Sulfide stress corrosion of some medium and low alloy steels. *Corrosion* **23**, 154–172 (1967).
31. Kane, R. D., Wilhelm, S. M. & Oldfield, J. W., Review of Hydrogen Induced Cracking of Steels in Wet H<sub>2</sub>S Refinery Service. in *International Conference on Interaction of Steels with Hydrogen in Petroleum Industry Pressure Vessel Service* (Materials Properties Council, 1989).
32. Craig, B. D. & Krauss, G. The structure of tempered martensite and its susceptibility to hydrogen stress cracking. *Metall. Trans. A* **11**, 1799–1808 (1980).
33. Craig, B., Brownlee, J. & Bruno, T. Sulfide stress cracking of nickel steels. *Corrosion* **48**, 90–97 (1992).
34. Lee, K.-H., Park, S.-g., Kim, M.-C., Lee, B.-S. & Wee, D.-M. Characterization of transition behavior in SA508 Gr.4N Ni–Cr–Mo low alloy steels with microstructural alteration by Ni and Cr contents. *Mater. Sci. Eng. A* **529**, 156–163 (2011).
35. ASTM A707/A707M-14, *Standard Specification for Forged Carbon and Alloy Steel Flanges for Low-Temperature Service* (ASTM International, 2014).
36. Walsh, F. & Price, S. in *Steel Forgings: Second Volume* Vol. STP16601S (eds Nisbett, E. G. & Melilli, A. S.) 196–209 (ASTM International, 1997).
37. Raabe, D. et al. Grain boundary segregation engineering in metallic alloys: A pathway to the design of interfaces. *Curr. Opin. Solid State Mater. Sci.* **18**, 253–261 (2014).
38. Bhadeshia, H. K. D. H. The bainite transformation: unresolved issues. *Mater. Sci. Eng. A* **273–275**, 58–66 (1999).
39. Fielding, L. C. D. The bainite controversy. *Mater. Sci. Technol.* **29**, 383–399 (2013).
40. Caballero, F. G., García-mateo, C., Capdevila, C. & Andrés, C. Gd Advanced Ultrahigh Strength Bainitic Steels. *Mater. Manuf. Process.* **22**, 502–506 (2007).
41. Cancio, M. J., Giacomel, B., Kissner, G., Valdez, M. & Vouilloz, F., High strength low alloy steel for HPHT wells. in *Offshore Technology Conference-Asia*, OTC-24746-MS, (Offshore Technology Conference, 25–28, 2014).
42. Randle, V. Grain boundary engineering: an overview after 25 years. *Mater. Sci. Technol.* **26**, 253–261 (2013).
43. King, A. H. & Shekhar, S. What does it mean to be special? The significance and application of the Brandon criterion. *J. Mater. Sci.* **41**, 7675–7682 (2006).
44. Bechtle, S., Kumar, M., Somerday, B. P., Launey, M. E. & Ritchie, R. O. Grain-boundary engineering markedly reduces susceptibility to intergranular hydrogen embrittlement in metallic materials. *Acta Mater.* **57**, 4148–4157 (2009).
45. Watanabe, T. Grain boundary engineering: historical perspective and future prospects. *J. Mater. Sci.* **46**, 4095–4115 (2011).
46. ISO 21457:2010, *Petroleum, Petrochemical And Natural Gas Industrie–Materials Selection and Corrosion Control For Oil and Gas Production Systems* (International Organization for Standardization, 2010).
47. Nešić, S. Key issues related to modelling of internal corrosion of oil and gas pipelines – A review. *Corros. Sci.* **49**, 4308–4338 (2007).
48. Bhavsar, R. B., Collins, A. & Silverman, S., Use of alloy 718 and 725 in oil and gas industry. in *Proceedings of the International Symposium: Superalloys 718, 625, 706 and Various Derivatives.*, 47–55 (The Minerals, Metals and Materials Society (TMS), 2001).
49. Malik, A. U., Siddiqi, N. A., Ahmad, S. & Andijani, I. N. The effect of dominant alloy additions on the corrosion behavior of some conventional and high-alloy stainless-steels in seawater. *Corros. Sci.* **37**, 1521–1535 (1995).
50. API 6ACRA, *Age-hardened Nickel-based Alloys for Oil and Gas Drilling and Production Equipment* (American Petroleum Institute, 2015).
51. Oradei-Basile, A. & Radavich, J. F., A current TTT diagram for wrought alloy 718. in *Proceedings of the International Symposium: Superalloys 718, 625 and Various Derivatives.*, 325–335 (The Minerals, Metals and Materials Society (TMS), 1991).
52. Rebak, R. B. et al. Effect of thermal treatment on the localized corrosion behavior of alloy 718 (UNS N07718). in *EUROCORR 2014*, 8–12 (European Federation of Corrosion, 2014).
53. Mannan, S. & Veltry, F. Time-temperature-transformation diagram of alloy 725. in *Proceedings of the International Symposium: Superalloys 718, 625, 706 and Various Derivatives.*, 345–356 (The Minerals, Metals and Materials Society (TMS), 2001).
54. Dong, J. X., Zhang, M. C. & Mannan, S. K. Microstructures and the structure stability of Inconel 725 a new age-hardenable corrosion resistant superalloy. *Acta Metall. Sin.* **16**, 145–150 (2003).
55. Jargelius-Pettersson, R. F. A. Application of the pitting resistance equivalent concept to some highly alloyed austenitic stainless steels. *Corrosion* **54**, 162–168 (1998).
56. Galliano, F. et al. Effect of trapping and temperature on the hydrogen embrittlement susceptibility of alloy 718. *Mater. Sci. Eng. A* **611**, 370–382 (2014).
57. Cassagne, T., Bonis, M. & Duret, C. Understanding field failures of alloy 718 forging materials in HP/HT wells. in *EUROCORR 2008*, 1–13 (European Federation of Corrosion, 7–11, September 2008).
58. Nice, P. et al. Hydrogen embrittlement failure of a precipitation hardened nickel alloy subsurface safety valve component installed in a North Sea seawater injection well. in *CORROSION*, 3892 (NACE International, 2014).
59. Shademan, S. S., Martin, J. W. & Davis, A. P. UNS N07725 Nickel Alloy Connection Failure. in *CORROSION*, C2012-0001095 (NACE International, 2012).
60. Osen, I. & Frydenberg, T. Nickel Alloy 725 Connection Failure: Root Cause Analysis Report. Report No. G1-VW-U-US00-C35-0419\_rev3, (General Electric, Sandvika, Norway, 2015).
61. Olden, V., Kvaale, P. E., Simensen, P. A., Aaldstedt, S. & Solberg, J. K. The Effect of PWHT on the material properties and micro structure in inconel 625 and inconel 725 Buttered Joints. in *22nd International Conference on Offshore Mechanics and Arctic Engineering*, OMAE2003-37196, 109–115 (ASME International, 2003).
62. Beaugrand, V. C., Smith, L. S. & Gittos, M. F. Subsea dissimilar joints: failure mechanisms and opportunities for mitigation. in *CORROSION*, 9305, 22–26 (NACE International, 2009).
63. API 5L, *Specification for Line Pipe* (American Petroleum Institute, 2013).
64. ASTM A694/A694M-16, *Standard Specification for Carbon and Alloy Steel Forgings for Pipe Flanges, Fittings, Valves, and Parts for High-Pressure Transmission Service* (ASTM International, 2016).
65. ASTM A182/182M, *Standard Specification for Forged or Rolled Alloy and Stainless Steel Pipe Flanges, Forged Fittings, and Valves and Parts for High-Temperature Service* (ASTM International, 2016).
66. Rosenqvist, F., Estrada, S. & Haeberle, T. GE Oil & Gas Quality Management System Engineering Welding Standard. Material Selection and Buttering Practices for Low Alloy Steel Flanges, Hubs, & Other Subsea Components to be Welded to Piping Without PWHT. Report No. QW-ENG-7.3.5-008, (General Electric, 2014).
67. Lippold, J. C. & Kotecki, D. J. *Welding Metallurgy and Weldability of Stainless Steels Ch. Duplex Stainless Steels*, 230–245 (Wiley, 2005).
68. Umekuni, A. & Masubuchi, K. Usefulness of undermatched welds for high-strength steels. *Weld. J.* **76**, S256–S263 (1997).
69. ASME ASME Boiler and Pressure Vessel Code. Section II. Part D: Properties (Metric) (Materials) (ASME International, 2009).
70. Hartbower, C. & Pellini, W. Explosion bulge test studies of the deformation of weldments. *Weld. J.* **30**, 3075–3185 (1951).
71. Mannan, M. A., Golihue, R., Kiser, S., McCoy, S. A. & Philipp, J., A new nickel alloy filler metal designed for welding high strength ID-clad steels. in *EUROCORR*, 50697, 11–15 (European Federation of Corrosion, 2016).
72. Vatne, J. & Verdolin, R., Difficulties In The Use Of NACE MR0175/ISO 15156. in *CORROSION*, 11112, 13–17 (NACE International, 2011).
73. Sagara, M. et al. Evaluation of Susceptibility to Hydrogen Embrittlement of High Strength Corrosion Resistant Alloys. in *CORROSION*, 7847, 6–10 (NACE International, 2016).
74. Denpo, K. & Ogawa, H. Crevice corrosion of corrosion-resistant alloys in sour environments. *Corrosion* **47**, 592–597 (1991).

75. Miyasaka, A., Denpo, K. & Ogawa, H. Environmental aspects of SCC of high alloys in sour environments. *Corrosion* **45**, 771–780 (1989).
76. Tsujikawa, S. et al. Alternative for evaluating sour gas resistance of low-alloy steels and corrosion-resistant alloys. *Corrosion* **49**, 409–419 (1993).
77. Cao, L., Anderko, A., Gui, F. & Sridhar, N. Localized corrosion of corrosion resistant alloys in H<sub>2</sub>S-containing environments. *Corrosion* **72**, 636–654 (2016).
78. Anderko, A., Cao, L., Gui, F., Sridhar, N. & Engelhardt, G. Modeling localized corrosion of corrosion-resistant alloys in oil and gas production environments: II. corrosion potential. *Corrosion* (2016).
79. Anderko, A., Gui, F., Cao, L., Sridhar, N. & Engelhardt, G. R. Modeling localized corrosion of corrosion-resistant alloys in oil and gas production environments: part i. repassivation potential. *Corrosion* **71**, 1197–1212 (2015).
80. Siegmund, G., Schmitt, G. & Kuhl, L., Unexpected Sour Cracking Resistance of Duplex and Superduplex Steels. in *CORROSION*, 7631, 6–10 (NACE International, 2016).
81. Yao, J., Dong, C., Man, C., Xiao, K. & Li, X. The electrochemical behavior and characteristic of passive film on 2205 duplex stainless steel under various hydrogen charging conditions. *Corrosion* **72**, 42–50 (2016).
82. Guo, L. Q. et al. Effect of hydrogen on pitting susceptibility of 2507 duplex stainless steel. *Corros. Sci.* **70**, 140–144 (2013).
83. Moon, S. M. & Pyun, S. I. The corrosion of pure aluminium during cathodic polarization in aqueous solutions. *Corros. Sci.* **39**, 399–408 (1997).
84. Pyun, S.-I., Lim, C. & Oriani, R. A. The role of hydrogen in the pitting of passivating films on pure iron. *Corros. Sci.* **33**, 437–444 (1992).
85. Thomas, S. et al. The effect of absorbed hydrogen on the dissolution of steel. *Heliyon* **2**, e00209 (2016).
86. Armacanqui, M. E. & Oriani, R. A. Technical note: effect of hydrogen on the pitting resistance of passivating film on nickel in chloride-containing solution. *Corrosion* **44**, 696–698 (1988).
87. Thomas, S., Sundararajan, G., White, P. D. & Biribilis, N. The effect of absorbed hydrogen on the corrosion of steels: review, discussion, and implications. *Corrosion* **73**, 426–436 (2017).
88. Djukic, M. B., Bakic, G. M., Zeravcic, V. S., Sedmak, A. & Rajcic, B. Hydrogen embrittlement of industrial components: prediction, prevention, and models. *Corrosion* **72**, 943–961 (2016).
89. Geng, W.-T., Freeman, A. J., Olson, G. B., Tateyama, Y. & Ohno, T. Hydrogen-promoted grain boundary embrittlement and vacancy activity in metals: insights from Ab initio total energy calculations. *Mater. Trans.* **46**, 756–760 (2005).
90. Paxton, A. T. & Katzarov, I. H. Quantum and isotope effects on hydrogen diffusion, trapping and escape in iron. *Acta Mater.* **103**, 71–76 (2016).
91. Tahir, A. M., Janisch, R. & Hartmaier, A. Hydrogen embrittlement of a carbon segregated  $\Sigma 5(310)[001]$  symmetrical tilt grain boundary in  $\alpha$ -Fe. *Mater. Sci. Eng. A* **612**, 462–467 (2014).
92. Deng, Y., Hajilou, D., Wan, D., Kheradmand, N. & Barnoush, A. In-situ micro-cantilever bending test in environmental scanning electron microscope: Real time observation of hydrogen enhanced cracking. *Scripta Mater.* **127**, 19–23 (2017).
93. Hajilou, T., Deng, Y., Rogne, B. R., Kheradmand, N. & Barnoush, A. In situ electrochemical microcantilever bending test: A new insight into hydrogen enhanced cracking. *Scripta Mater.* **132**, 17–21 (2017).
94. Barnoush, A., Asgari, M. & Johnsen, R. Resolving the hydrogen effect on dislocation nucleation and mobility by electrochemical nanoindentation. *Scripta Mater.* **66**, 414–417 (2012).
95. Barnoush, A. & Vehoff, H. Recent developments in the study of hydrogen embrittlement: Hydrogen effect on dislocation nucleation. *Acta Mater.* **58**, 5274–5285 (2010).
96. Tal-Gutelmacher, E., Gemma, R., Volkert, C. A. & Kirchheim, R. Hydrogen effect on dislocation nucleation in a vanadium (100) single crystal as observed during nanoindentation. *Scripta Mater.* **63**, 1032–1035 (2010).
97. Nibur, K., Bahr, D. & Somerday, B. Hydrogen effects on dislocation activity in austenitic stainless steel. *Acta Mater.* **54**, 2677–2684 (2006).
98. Golovin, Y. I. Nanoindentation and mechanical properties of solids in sub-microvolumes, thin near-surface layers, and films: A Review. *Phys. Solid State* **50**, 2205–2236 (2008).
99. Nili, H., Kalantar-zadeh, K., Bhaskaran, M. & Sriram, S. In situ nanoindentation: Probing nanoscale multifunctionality. *Progress Mater. Sci.* **58**, 1–29 (2013).
100. Franke, O. et al. Incipient plasticity of single-crystal tantalum as a function of temperature and orientation. *Philos. Mag.* **95**, 1866–1877 (2014).
101. Lodes, M. A., Hartmaier, A., Göken, M. & Durst, K. Influence of dislocation density on the pop-in behavior and indentation size effect in CaF<sub>2</sub> single crystals: Experiments and molecular dynamics simulations. *Acta Mater.* **59**, 4264–4273 (2011).
102. Montagne, A., Audurier, V. & Tromas, C. Influence of pre-existing dislocations on the pop-in phenomenon during nanoindentation in MgO. *Acta Mater.* **61**, 4778–4786 (2013).
103. Sekido, K., Ohmura, T., Hara, T. & Tsuzaki, K. Effect of Dislocation Density on the Initiation of Plastic Deformation on Fe&ndash;C Steels. *Mater. Trans.* **53**, 907–912 (2012).
104. Wu, D., Jang, J. S. C. & Nieh, T. G. Elastic and plastic deformations in a high entropy alloy investigated using a nanoindentation method. *Intermetallics* **68**, 118–127 (2016).
105. Wu, D., Morris, J. R. & Nieh, T. G. Effect of tip radius on the incipient plasticity of chromium studied by nanoindentation. *Scripta Mater.* **94**, 52–55 (2015).
106. Jian, S.-R. & Juang, J.-Y. Nanoindentation-induced pop-in effects in GaN thin films. *IEEE Trans. Nanotechnol.* **12**, 304–308 (2013).
107. Oliver, W. C. & Pharr, G. M. Measurement of hardness and elastic modulus by instrumented indentation: Advances in understanding and refinements to methodology. *J. Mater. Res.* **19**, 3–20 (2004).
108. Chen, Y. Z. et al. Increase in dislocation density in cold-deformed Pd using H as a temporary alloying addition. *Scripta Mater.* **68**, 743–746 (2013).
109. Kirchheim, R. Reducing grain boundary, dislocation line and vacancy formation energies by solute segregation. I. Theoretical background. *Acta Mater.* **55**, 5129–5138 (2007).
110. Kirchheim, R. On the solute-defect interaction in the framework of a defectant concept. *Int. J. Mater. Res.* **100**, 483–487 (2009).
111. Kirchheim, R. Solid solution softening and hardening by mobile solute atoms with special focus on hydrogen. *Scripta Mater.* **67**, 767–770 (2012).
112. Bamoush, A., Kheradmand, N. & Hajilou, T. Correlation between the hydrogen chemical potential and pop-in load during in situ electrochemical nanoindentation. *Scripta Mater.* **108**, 76–79 (2015).
113. Zamanzade, M., Vehoff, H. & Barnoush, A. Cr effect on hydrogen embrittlement of Fe<sub>3</sub>Al-based iron aluminide intermetallics: Surface or bulk effect. *Acta Mater.* **69**, 210–223 (2014).
114. Greer, J. R., Oliver, W. C. & Nix, W. D. Size dependence of mechanical properties of gold at the micron scale in the absence of strain gradients. *Acta Mater.* **53**, 1821–1830 (2005).
115. Kiener, D., Motz, C., Dehm, G. & Pippan, R. Overview on established and novel FIB based miniaturized mechanical testing using in-situ SEM. *Int. J. Mater. Res.* **100**, 1074–1087 (2009).
116. Kiener, D., Motz, C., Rester, M., Jenko, M. & Dehm, G. FIB damage of Cu and possible consequences for miniaturized mechanical tests. *Mater. Sci. Eng. A* **459**, 262–272 (2007).
117. Kiener, D., Motz, C., Schöberl, T., Jenko, M. & Dehm, G. Determination of Mechanical Properties of Copper at the Micron Scale. *Adv. Eng. Mater.* **8**, 1119–1125 (2006).
118. Schneider, A. S. et al. Influence of bulk pre-straining on the size effect in nickel compression pillars. *Mater. Sci. Eng. A* **559**, 147–158 (2013).



**Open Access** This article is licensed under a Creative Commons Attribution 4.0 International License, which permits use, sharing, adaptation, distribution and reproduction in any medium or format, as long as you give appropriate credit to the original author(s) and the source, provide a link to the Creative Commons license, and indicate if changes were made. The images or other third party material in this article are included in the article's Creative Commons license, unless indicated otherwise in a credit line to the material. If material is not included in the article's Creative Commons license and your intended use is not permitted by statutory regulation or exceeds the permitted use, you will need to obtain permission directly from the copyright holder. To view a copy of this license, visit <http://creativecommons.org/licenses/by/4.0/>.

© The Author(s) 2017